THE ASTROPHYSICAL JOURNAL, 472:711–722, 1996 December 1

THE CHEMICAL ABUNDANCES OF THE HYDROGEN-POOR PLANETARY NEBULAE A30 AND A58

M. A. GUERRERO[1] AND A. MANCHADO[1]
Instituto de Astrofisica de Canarias, E-38200 La Laguna (Tenerife), Spain; mar@ll.iac.es
Received 1996 March 25; accepted 1996 June 25

ABSTRACT

We present new CCD narrowband images and spatially resolved intermediate-dispersion spectroscopy of the hydrogen-poor nebulae A30 and A58. These data have allowed us to obtain information on the physical properties and chemical abundances of the inner knots and outer envelopes of A30 and A58 as a basis for the discussion of their implications in the evolutionary theories. In particular, hydrogen emission from the central knots has been carefully measured, and, consequently, the rates of conversion of hydrogen into helium have been established with accuracy. The rates found indicate that almost all the original hydrogen (between 75% and 95%) has been burned into helium. The chemical segregation among the knots of A30 previously suggested by Jacoby & Ford is confirmed. The A58 inner knot, which is spatially resolved in two different components, shows evidence of excitation by shocks. Helium abundances and the N/O ratio in the outer envelope of this nebula are very high, therefore indicating that the nebula formed as the result of the evolution of an intermediate-mass star.

An analysis of the chemical abundances, including other objects of the same class, gives some hints that He/H and O/H are anticorrelated. The time elapsed between the formation of the outer envelopes and the ejection of the central knots also seems to be related to the central knots' chemical abundances.

Subject headings: ISM: abundances — planetary nebulae: individual (A30, A58) — stars: AGB and post-AGB

1. INTRODUCTION

Planetary nebulae (PNs) with hydrogen-rich outer envelopes, surrounding hydrogen-deficient inner knots, compose one of the most singular classes among PNs. Only five objects are currently members of such an exotic group: IRAS 18333−2357 in the globular cluster M22 (Gillett et al. 1986), A78 (Jacoby & Ford 1983, hereafter JF83), IRAS 15154−5258 (Manchado, García-Lario, & Pottasch 1989), and the two PNs studied in this paper, A30 (PNG 208.5+33.2) and A58 (PNG 037.5−05.1).

A30 is a large, round, and presumably old PN whose outer envelope is shown through narrowband filter images in the Hα + [N II] and [O III] light as a limb-brightened nebula extending ∼130″ (Fig. 1 [Pl. 13]). In addition, it exhibits hydrogen-deficient central knots (JF83) discovered simultaneously by Jacoby (1979) and Hazard et al. (1980). These knots have been interpreted as a clumpy expanding disk or ring structure and two polar knots that are being swept up by the fast stellar wind (Harrington 1986; Jacoby & Chu 1989).

The hydrogen-poor nature of the central knot of A58 (Fig. 1) was first suggested by Pottasch et al. (1986). The observations of Seitter (1987) confirmed this point, the spectrum of the central knot of A58 pointing to a complete lack of Hα, with the emission lines slightly blueshifted with respect to the nebular emission lines.

From an evolutionary point of view, such peculiar objects are commonly interpreted as old PNs whose central stars have experienced a secondary ejection of highly processed material that forms the observed inner knots. In order to explain this behavior, which clearly departs from standard stellar evolution on the post–asymptotic giant branch (post-AGB), Iben et al. (1983) proposed an alternative evolutionary path. According to their views, a subset of hydrogen-burning, low-mass PN nuclei (PNNs)—which they named "born-again AGB stars"—experience a late thermal pulse during the post-AGB phase and return to the AGB phase. At this stage, a second "superwind" phase may strip the envelope of the born-again AGB star, reaching regions where hydrogen has been depleted almost completely. After a few thousand years, such a star would evolve back again, but as a helium-burning PNN. A shell of highly processed material encircles it.

More recently, Soker & Livio (1994) proposed an alternative scenario. Under certain conditions, matter from an evolved nebula can flow back, once the stellar wind has ceased, to undergo accretion by the compact central star. If the accretion process continues for a sufficient time, the material will burn and produce a late helium flash.

As a basis for discussing the implications of hydrogen-poor PNs in the evolutionary theories in the AGB and post-AGB phases, we present new CCD narrowband images and spatially resolved intermediate-dispersion spectroscopy of the hydrogen-poor nebulae A30 and A58. In § 2 we describe the observations. The study of the physical properties and chemical abundances of the central knots and nebular material of A30 and A58 is in §§ 3 and 4, respectively. A discussion of the material presented in this paper is given in § 5. Finally, a summary is given in § 6.

2. OBSERVATIONS AND DATA REDUCTION

2.1. *Imagery*

The CCD images of A30 (Fig. 1) were obtained in the framework of the IAC Survey of Northern Planetary Nebulae (Manchado et al. 1996). The 82 cm IAC80 telescope at the Teide Observatory (Tenerife) was used with a

[1] Visiting Astronomer, German-Spanish Astronomical Centre, Calar Alto, operated by the Max-Planck-Institut für Astronomie, Heidelberg, jointly with the Spanish National Commission for Astronomy.

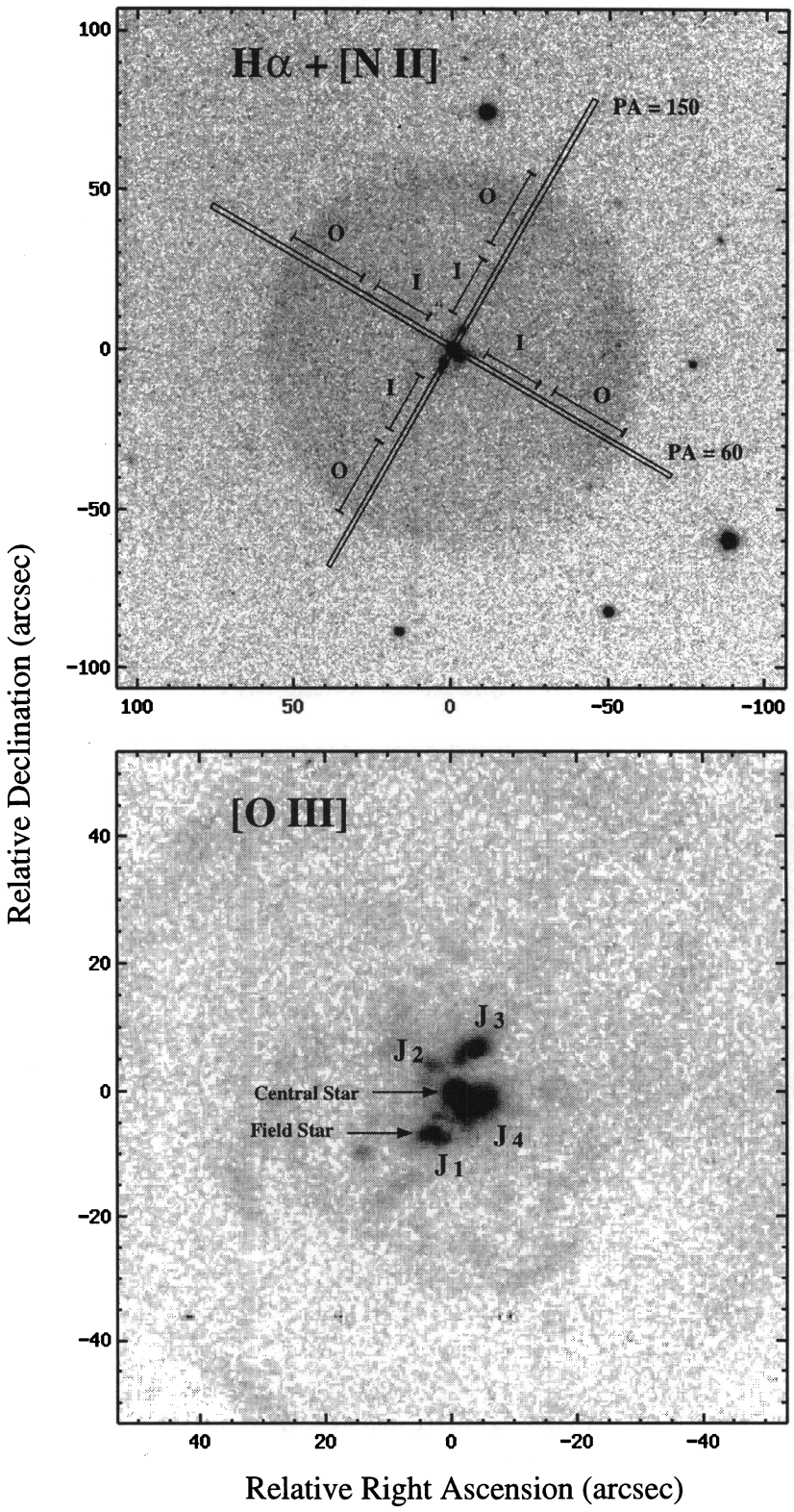

FIG. 1.—CCD images of A30 through narrowband filters in the Hα + [N II] (*top*) and [O III] (*bottom*) light. The slit positions, as well as the extension of the apertures considered in the envelope, are shown on the Hα + [N II] image. The central knots are labeled on the [O III] image.

GUERRERO & MANCHADO (see 472, 711)

1024 × 1024 pixel^2 Thomson CCD with pixel size 0.″435. Two narrowband interference filters made it possible to isolate the Hα + [N II] and [O III] lines, respectively. Their FWHMs are 100 and 30 Å, respectively. Four 15 minute exposure time frames were obtained and subsequently combined to obtain the images shown in Figure 1.

The CCD images of A58 (Fig. 2 [Pl. 14]) were obtained with the 2.56 m Nordic Optical Telescope (NOT) on 1995 July 3 at the Roque de los Muchachos Observatory on the island of La Palma (Spain). The images were acquired through narrowband interference filters (FWHM $\lesssim$ 9 Å) in the Hα and [N II] λ6584 lines. The contribution of each line to the other is negligible. A 1024 × 1024 pixel^2 Thomson CCD with pixel size 0.″139 and field ∼140″ was used.

Figures 1 and 2 show A30 and A58 as two classical PNs, with low surface brightness and limb-brightened appearance. If we exclude the central regions, the Hα + [N II] image of A30 shows a smooth, round nebula. In the case of A58, its shape gives some evidence to support interaction with the surrounding medium, with material apparently compressed toward the western parts. In addition, the central star is slightly (∼0.″6) displaced west of the nebula. An enlarged image of the central knot is also shown in Figure 2. Extended emission is found toward the southwestern part of the central knot.

2.2. *Intermediate Dispersion Spectroscopy*

Long-slit spectral data of A30 were collected at the 3.6 m telescope at the La Silla Observatory (Chile) from 1986 February 2 to February 4, using the ESO Faint Object Spectrograph and Camera (EFOSC) with the RCA ESO CCD 3 (330 × 512 pixels). The slit was 1.″5 wide and 3.′7 long. Observations of A58 were performed at the Calar Alto Observatory's (CAHA) 3.5 m telescope (Almería, Spain) on 1994 July 26–28. Long-slit intermediate-dispersion spectra were secured by means of the Twin Cassegrain Spectrograph (TCS) with two CCD detectors (Tektronix 1024 × 1024 pixels) operating simultaneously. The slit was 1.″2 wide and 4′ long. Instrument settings are listed in Table 1, including information about the telescopes, chips, instruments, and grisms used and the spectral ranges, reciprocal dispersions, and spatial resolutions achieved.

We observed A30 at two slit positions in order to obtain information about the different inner knots, the central star, and the outer envelope. In A58 the long slit was placed across the central star and knot. A journal of the spectroscopic observations is reported in Table 2. Slit positions are shown in Figures 1 and 2.

Data reduction was carried out at the IAC using the standard software package IRAF.[2] The spectral images were bias-subtracted and trimmed, flat-field–corrected, and cleaned of cosmic rays. Wavelength calibration and distortion correction were performed with polynomial fits to the He-Ar arc lamps. Later, sky subtraction was carried out using the parts of the images free from nebular emission; the spectra were corrected for continuous atmospheric extinction with appropriate extinction curves for each observatory. Finally, absolute flux calibration was performed by means of observations of the standard stars BD +08°2015 (Stone 1977), Ross 627 (Oke 1974), and Feige 110 (Oke 1990). Once one-dimensional spectra of the interesting regions had been extracted, fluxes were measured using the FITLINES IRAF-IAC task developed by J. Acosta. This program makes it possible to estimate the errors involved in flux measurements assuming that the flux is affected by Poisson counting statistics.

3. A30

In the following discussion, we will adopt Jacoby's notation for the knots, which enumerates them clockwise, namely, J1 (knot at position angle 150°), J2 (P.A. 59°), J3 (P.A. 330°), and J4 (P.A. 237°). They appear labeled in Figure 1 (*bottom*) for clarity. According to Jacoby & Chu

[2] IRAF is distributed by the National Optical Astronomy Observatories, which is operated by the Association of Universities for Research in Astronomy, Inc. (AURA), under cooperative agreement with the National Science Foundation.

TABLE 1

INSTRUMENTAL SET OF THE SPECTROSCOPIC OBSERVATIONS

Instrumental Set Key	Telescope	Instrument	Grism	Spectral Range (Å)	Reciprocal Dispersion (Å pixel^{-1})	Spatial Resolution (arcsec pixel^{-1})
A	3.6 m ESO	EFOSC	B150	3650–5450	3.90	0.675
B.....	3.6 m ESO	EFOSC	O150	5050–6850	3.90	0.675
C	3.5 m CAHA	TCS	T08	3650–5450	1.76	0.90
D	3.5 m CAHA	TCS	T04	5500–7350	1.80	0.90

TABLE 2

JOURNAL OF SPECTROSCOPIC OBSERVATIONS

Object	Date	Slit Position	Slit P.A. (deg)	Offset (arcsec)	Instrumental Set	Exposure Time (s)
A30.....	1986 Feb	1	60	0	A	1200
		1			B	1200
		2	150	0	A	1200
		2			B	1200
A58.....	1993 Jul	1	90	0	C	2000
		1			D	1800

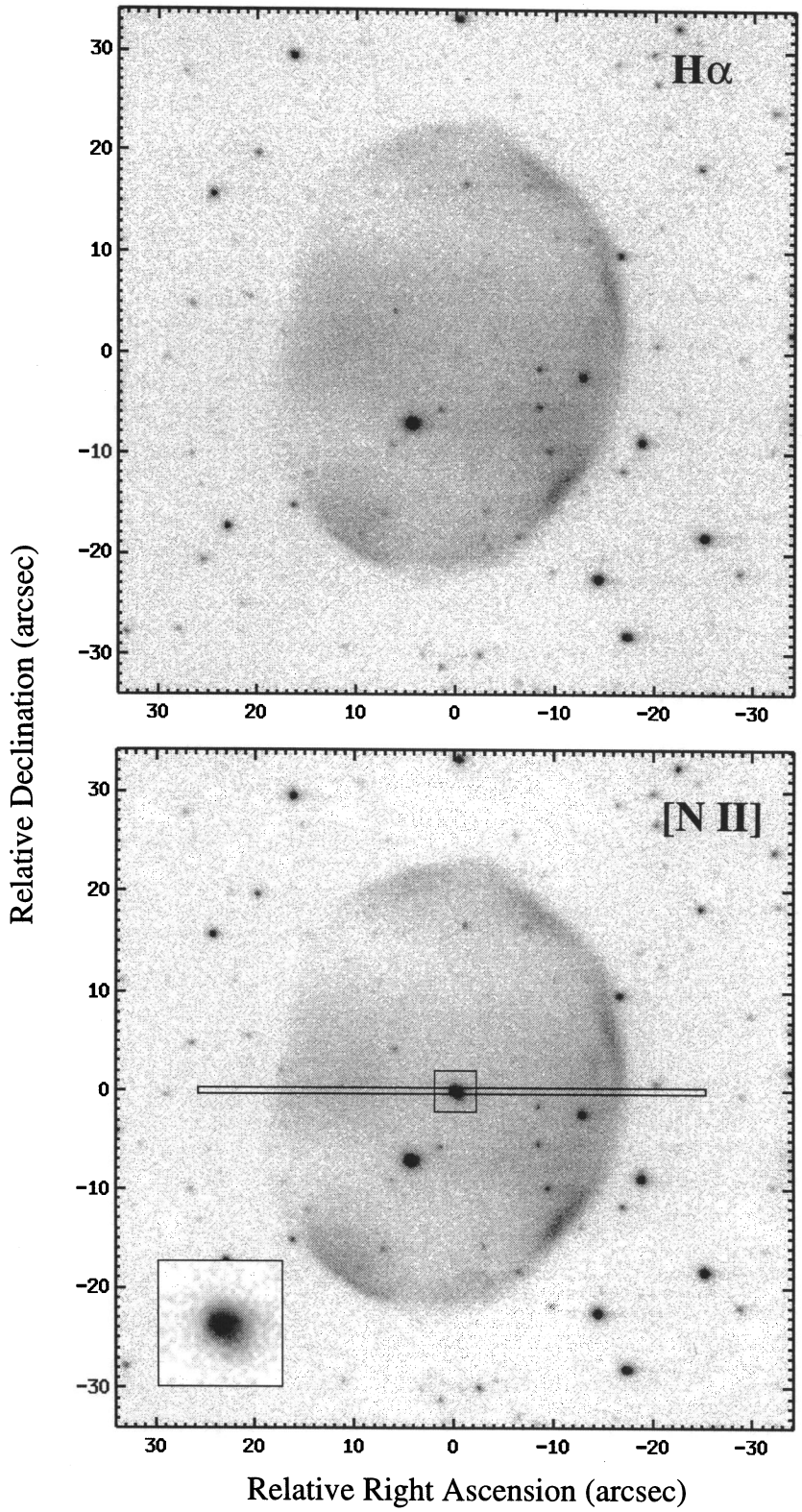

FIG. 2.—CCD images of A58 through narrowband filters in the Hα (*top*) and [N II] (*bottom*) light. The slit position is shown on the [N II] image. The central square 4″ × 4″ is shown enlarged on the bottom left-hand corner to show in detail the central knot. Emission extends toward the southwestern part ~1.″3 away.

(1989), knots J1 and J3 are the polar knots, whereas J2 and J4 are located at the equator, forming an expanding ring.

3.1. *Spectral Analysis*

We observed A30 at two slit positions, both passing across the central star. The slit at P.A. 150° passes over knots J1 and J3, while the slit at P.A. 60° covers the knots J2 and J4. Individual spectra were extracted for all four knots, the envelope, and the central star, and are shown in Figures 3 and 4. Emission from the envelope and from the central star are present in both two-dimensional spectra corresponding to the two slit positions. We averaged the one-dimensional spectra of each one of these regions to improve the signal-to-noise ratio.

In all the spectra of the inner knots, the contribution from the surrounding nebula has been removed by carefully analyzing the spatial profiles of the emission lines and fitting a continuum. These one-dimensional spectra (Fig. 3) show that forbidden lines from heavy elements and helium recombination lines are several times stronger than Hα, while Hβ was only observed in knots J1 and J3.

As for the outer envelope, although the Hα + [N II] images present a highly uniform surface brightness (except in the bright knots within 10″ of the central star), the [O III] image reveals the presence of knots and loops forming an inner shell halfway out to the outer shell. In order to analyze the spectroscopic information, the nebular envelope has been separated into two different regions (Fig. 1, *top*). The inner part of the surrounding nebula extends from 10″ up to 30″ from the central star, while the outer part of the envelope extends from 35″ to 60″ from the central star. Spectra from these regions are similar to those of other high-excitation PNs. Only Hα, Hβ, He II λ4686, and the [O III] lines λλ4959, 5007 are detected. Neither He I nor forbidden lines from low ionization stages, usually seen in other PNs (e.g., [O II], [N II]), appear in the spectra, thus indicating a high excitation. In fact, I(He II λ4686)/I(Hβ) ~ 1.2. It is also noticeable that the ratio between [O III] emission and Hβ decreases by a factor of 3 from the inner to the outer envelope.

The normalized spectrum of the central star, shown in Figure 5, is dominated by heavy lines of C IV (λλ5801, 5812, 4658, and λ6198) and O VI (the double feature λλ3811, 3834 and λ5290). Lines of N V (λλ4603, 4619) and N III (λλ4634, 4640, 4641) are also present, but they do not exhibit broad emissions. In agreement with Heap (1982), it can be classified as an O VI star, but with a composite spectrum of WC3 and WN2. The He II Pickering series appears in absorption (λλ5411, 4859, 4542, 4339, 4200, 4100), except for the line λ6560, which is in emission. As discussed below (§ 3.3), it is a hot star, with $T_{\rm eff}$ ~ 100,000 K.

3.2. *Line Intensity Ratios*

The measured line intensity ratios and the Hα and [O III] λ5007 fluxes are shown in Table 3. Owing to the uncertainties in the Hβ and Hα lines in the inner knots, line

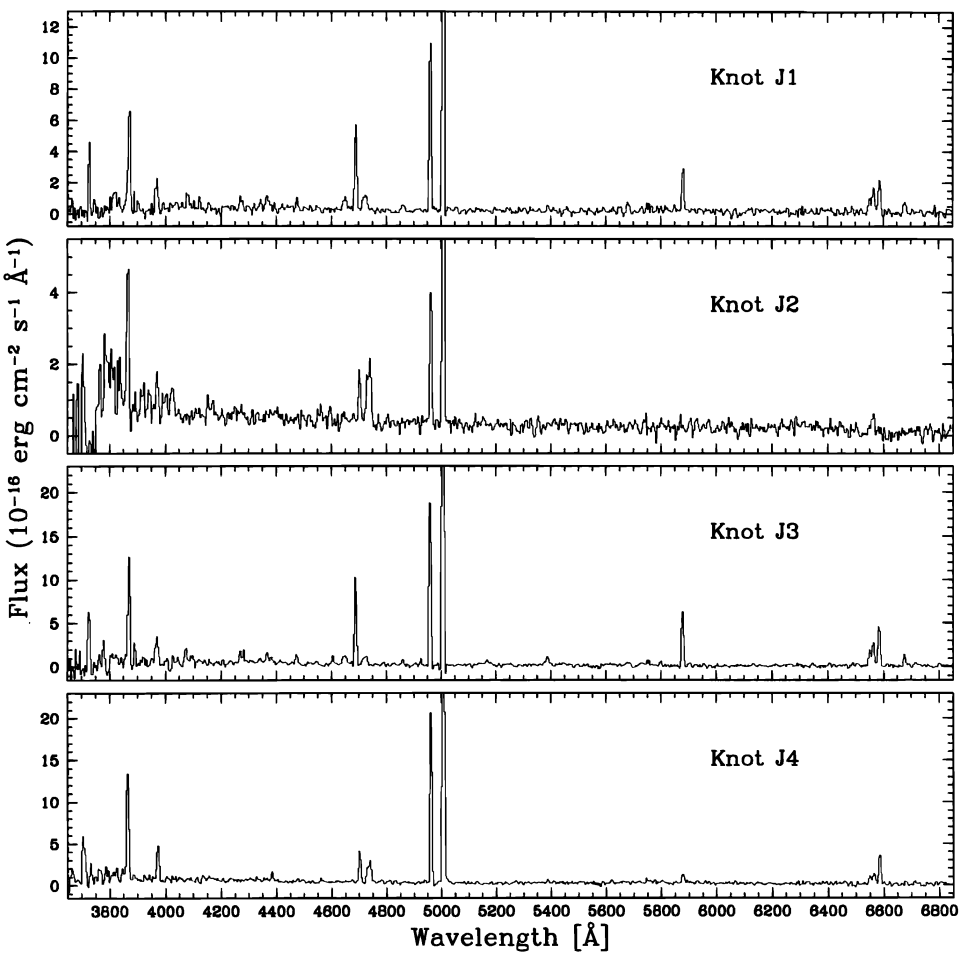

FIG. 3.—Individual spectra of the four central knots in A30. As described in the text, we used the notation for the knots introduced by Jacoby (1979).

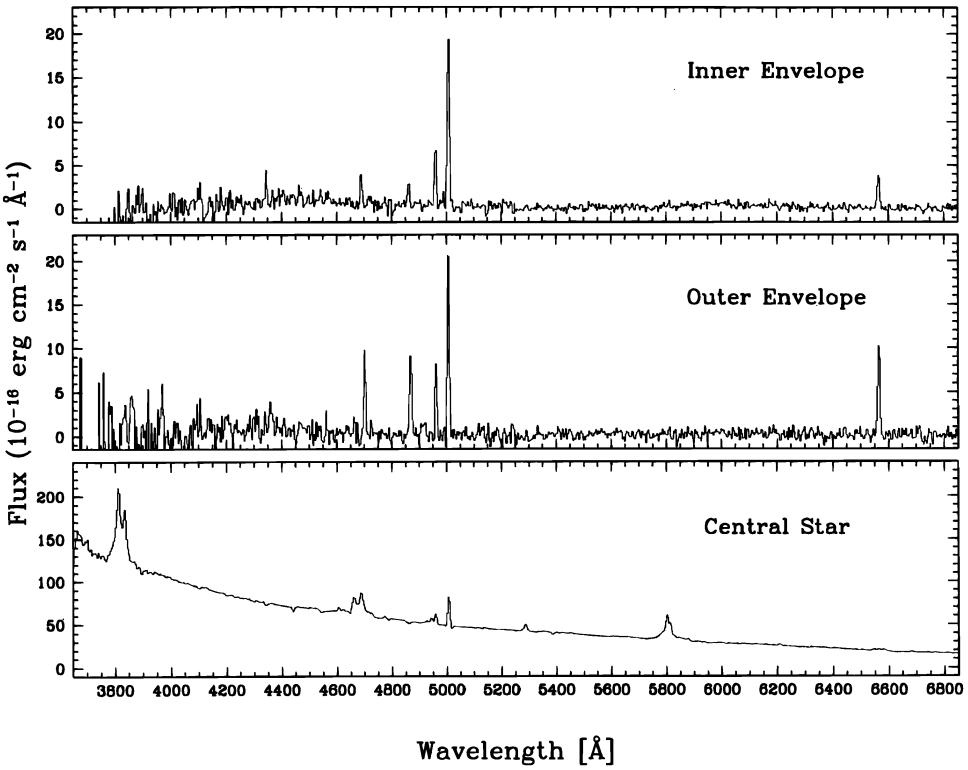

FIG. 4.—Individual spectra of the inner and outer envelopes, and of the central star in A30

strengths are tabulated relative to the intensity of [O III] λ5007 (= 1000).

Before performing any further analysis, we must consider the contribution of the He II Pickering series to the hydrogen Balmer series, since our spectral resolution is insufficient to resolve these lines separately. This usually amounts to a very small correction in PNs; however, in the knots' spectra, where He II λ4686 is very strong, an important

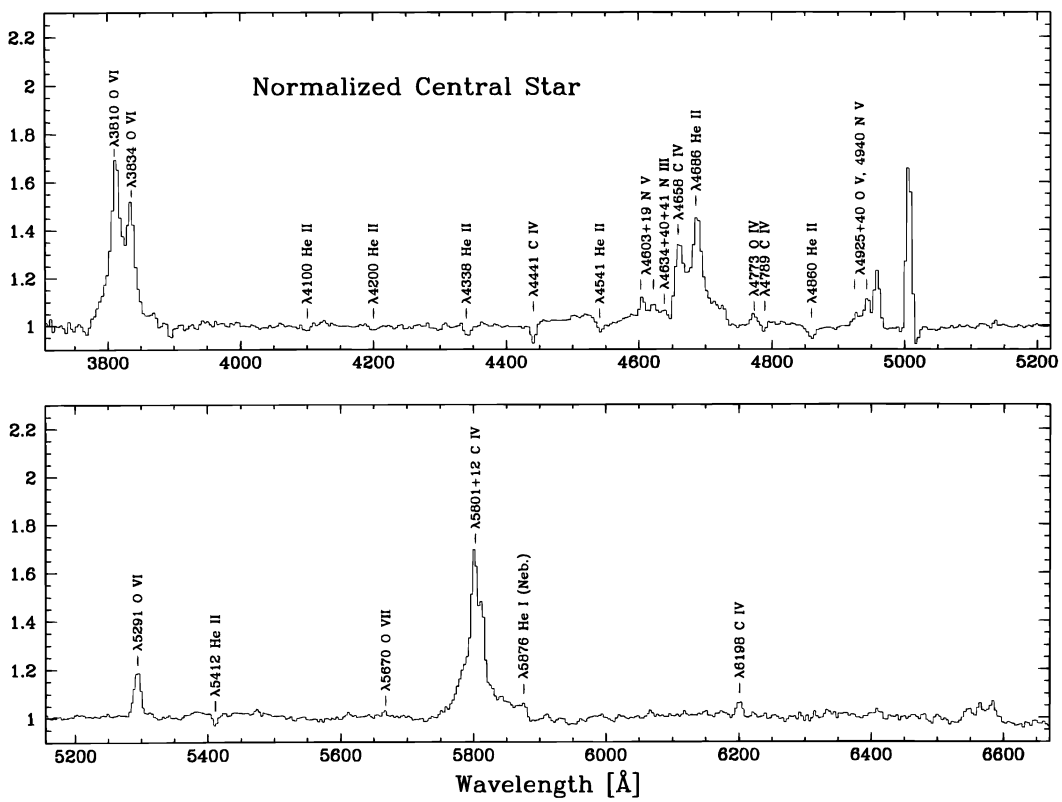

FIG. 5.—Normalized spectrum of the central star in A30. Stellar features have been marked. The strong O VI and C IV lines are noticeable.

TABLE 3

MEASURED LINE INTENSITY RATIOS FOR A30

Line	Knot 1	Knot 2	Knot 3	Knot 4	Inner	Outer
[O II] λ3727	129 ± 7	...	148 ± 14	122 ± 9	...	...
[Ne III] λ3869	270 ± 11	452 ± 21	253 ± 10	235 ± 5	...	...
Hε + [Ne III] + He I λ3970	80 ± 9	125 ± 15	85 ± 9	75 ± 5	...	...
[S II] λ4072	32 ± 6	...	39 ± 10	...	...	...
C II λ4267	32 ± 6	...	...	...	...	...
[O III] λ4363	44 ± 13	...	26 ± 7	15.9 ± 2.8	...	...
He I λ4471	21 ± 6	...	17.3 ± 4.4	...	...	...
[C III] λ4647	41 ± 7	...	35 ± 5	...	...	...
He II λ4686	200 ± 9	154 ± 22	181 ± 3	63 ± 3	191 ± 20	499 ± 50
[Ne IV] λ4715	31 ± 10	127 ± 24	15 ± 9	31 ± 3	...	...
[Ne IV] λ4725	35 ± 10	172 ± 24	21 ± 14	44 ± 4	...	...
Hβ λ4861	7.2 ± 4.7	...	3.6 ± 4.2	...	174.21	432 ± 53
[O III] λ4959	392 ± 5	341 ± 14	347 ± 3	318 ± 2	320 ± 21	359 ± 45
[O III] λ5007	1000	1000	1000	1000	1000	1000
He II λ5411	25 ± 6	...	31 ± 6	...	...	...
He I λ5876	103 ± 5	...	114 ± 4	20.7 ± 3.0	...	...
[N II] λ6548	39 ± 6	...	38 ± 3	19.3 ± 2.4	...	...
Hα λ6563	34 ± 8	50 ± 20	32 ± 4	16.9 ± 3.6	305 ± 17	936 ± 52
[N II] λ6584	86 ± 10	...	97 ± 5	65 ± 5	...	...
H I λ6678	35 ± 5	...	28.2 ± 2.9	6.3 ± 2.8	...	...
[S II] λ6717+31	...	...	12.6 ± 3.8	...	...	...
F(Hα)[a]	9.2	5.1	15.2	9.2	55.5	123
F([O III] λ5007)[a]	271	103	476	548	182	131

[a] Dereddened fluxes in units of 10^{-16} ergs cm^{-2} s^{-1}.

fraction of the measured Hβ and Hα flux might be due to contributions of the He II λλ4860, 6560 Pickering lines, respectively. The theoretical ratios of the flux of these lines to the known flux of He II λ4686[3] (Hummer & Storey 1987), $I4860 = 0.052I(4686)$ and $I6560 = 0.136I(4686)$, allowed us to compute the fraction of the λλ4861, 6563 emission due to He II lines.

Intensity ratios of the Hα and Hβ lines in Table 3 have been corrected for this effect. For Hα, the contribution of He II λ6560 is 47%, 30%, 43%, and 34% of the total flux measured at this wavelength in knots J1 to J4, respectively. Figure 6 shows a spatial profile brightness of the Hα line at the two slit positions, once the contribution from the line He II λ6560 has been removed. The absorption corresponds to the stellar position, since He II λ4686 is a strong feature of

[3] It is also possible to scale these fluxes to the He II λ5411 Pickering line, but this is much fainter than the line λ4686, and therefore we have preferred the latter. In any case, corrections from both lines are in agreement within the errors.

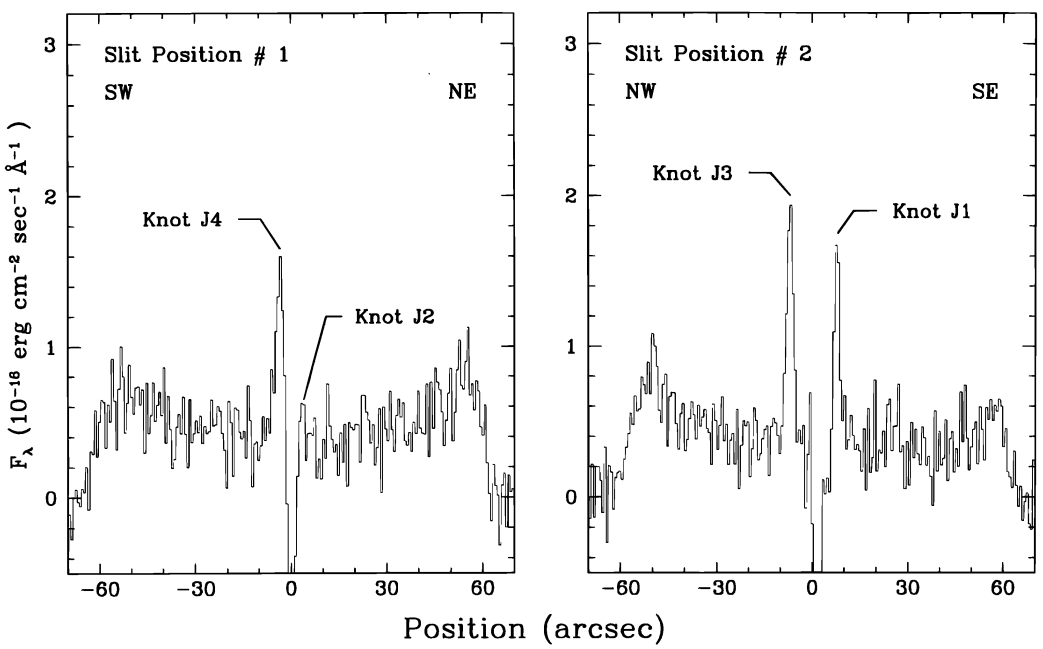

FIG. 6.—Brightness profile of the Hα line at the central knots position in A30. The two slit positions cover the four knots in the nebula. The continuum has been subtracted as described in the text.

the stellar spectrum. The positions of the various knots have been marked in Figure 6.

Extinction correction is a puzzling question in A30. As far as the surrounding nebula is concerned, no extinction correction was applied, according to the comparison of the measured and theoretical (Brocklehurst 1971) Hα/Hβ ratio.

This is in agreement with the reddening H I maps of Burstein & Heiles (1982). In the central knots, the uncertainty in the flux measurement of the Hβ line does not allow a reliable determination of the extinction. Cohen et al. (1977) reported some extinction at the central star position [$E(B-V) = 0.30$]. In this respect, the presence of dust-rich material surrounding the central region of A30 (Dinerstein & Lester 1984; Borkowski et al. 1994) may explain the existence of extinction inside the nebula. According to our data, there is no indication of extinction in the central region, therefore no extinction correction was applied.

3.3. *Physical Properties and Chemical Abundances*

Electron temperature, density, and ionic abundances were computed from the line strengths using a program that solves the statistical equilibrium equations for a 5 level atom, written by Preite-Martinez. This program makes use of the atomic constants listed by Mendoza (1983) and a few more recent values (e.g., the Ne^{++} collision strengths of Butler & Mendoza 1984). The elemental abundances were calculated according to the formulism of ionization correction factors (Kingsburgh & Barlow 1994). Helium abundances are derived with the correction of collisional effects (Clegg 1987).

We first consider the inner knots. We derived the electron temperature from the ratio between the [O III] auroral line λ4363 and the nebular lines $\lambda\lambda$4959, 5007. Since the auroral line is faint, its measurement has severe uncertainties. In knot J4, where λ4363 has the lowest error, a value of 14,000 $\pm$ 1000 K was deduced, while in knots J1 and J3 the temperature seems to be higher (17,000–19,000 K). Because the error which affects these lines is higher, we will use the value inferred for knot J4 for the other inner knots. This value is in agreement with the value derived by JF83 and Kingsburgh & Barlow (1994). An estimate of the electron density can be obtained if the distance to the nebula and the flux of a recombination line are known. Although the Hβ line flux is usually employed for this purpose, it is obviously more useful in this case to use the line He II λ4686. We can then use expression (5) of JF83,

$$N_e(\mathrm{rms}) = \frac{8 \times 10^{21}}{r^3 d} F(4686)\left(\frac{N_{H^+}}{N_{He^{++}}} + \frac{N_{He^+}}{N_{He^{++}}} + 2\right), \quad (1)$$

where $F(4686)$ is in units of ergs cm^{-2} s^{-1}, r is the angular radius in arcseconds, d is the distance in parsecs, and the electron temperature is 15,000 K. We adopted the same initial assumptions for the ionic abundances as in JF83. Once they were determined, we began an iteration process, obtaining the values listed in Table 4. Distance was set at 1.7 kpc (Cahn, Kaler, & Stanghellini 1992), and the angular sizes of each knot were taken from Borkowski et al. (1993). An estimate of the masses of each knot has also been included in Table 4. A density contrast is apparent between the denser polar knots J1 and J3 and the equatorial knots J2 and J4.

The chemical abundances of the knots are summarized in Table 4. The most remarkable fact is the high ratio of He/H, which rises up to 7 in knots J1 and J3 (the polar knots) and is slightly lower in knot J4 (He/H $\sim$ 4). If we assume that helium has not been converted into carbon and oxygen, the present amount of helium is the sum of the initial helium plus the newly created helium, which is a quarter of the difference between the initial and final number of hydrogen

TABLE 4

ABUNDANCES OF A30

Plasma Diagnostics and Chemical Abundances	Knot 1	Knot 2	Knot 3	Knot 4
t[O III]	1.4[a]	1.4[a]	1.4[a]	1.4 $\pm$ 0.1
N_e (cm^{-3})	2100	120	2700	250
M ($\times 10^5$ $M_\odot$)	2.7	6.8	3.4	12.4
$O^{++}/H^+ \times 10^4$	11.0 $\pm$ 1.8	7.5 $\pm$ 1.3	11.6 $\pm$ 1.9	22.3 $\pm$ 3.6
$O^+/H^+ \times 10^4$	1.7 $\pm$ 0.4	...	2.1 $\pm$ 0.6	3.3 $\pm$ 0.8
O/H $\times 10^4$	15.2 $\pm$ 3.8	...	16.3 $\pm$ 3.7	32.5 $\pm$ 8.8
$N^+/H^+ \times 10^5$	6.6 $\times$ 1.5	...	7.8 $\pm$ 1.3	10 $\pm$ 2
N/H $\times 10^5$	59	...	62	100
$S^+/H^+ \times 10^7$	...	...	19 $\pm$ 7	...
S/H $\times 10^7$	...	...	170	...
$Ne^{++}/N^+ \times 10^4$	5.6 $\pm$ 1.2	33 $\pm$ 11	23.2 $\pm$ 4.7	48 $\pm$ 11
Ne/N $\times 10^4$	7.7	...	7.8	14.4
He^+/H^+ (4471)	3.8 $\pm$ 2.0	...	3.2 $\pm$ 1.2	...
He^+/H^+ (5876)	6.9 $\pm$ 1.7	...	8.0 $\pm$ 1.2	2.8 $\pm$ 0.9
He^+/H^+ (6678)	7.3 $\pm$ 2.6	...	6.2 $\pm$ 1.4	2.7 $\pm$ 1.6
He^+/H^+ (average)	5.9 $\pm$ 1.2	...	5.8 $\pm$ 0.7	2.8 $\pm$ 0.7
He^{++}/H^+	1.8 $\pm$ 0.5	1.0 $\pm$ 0.5	1.7 $\pm$ 0.3	1.2 $\pm$ 0.3
He/H	7.7 $\pm$ 1.7	...	7.5 $\pm$ 1.0	4.0 $\pm$ 1.0
N^+/O^+	$0.39^{+0.19}_{-0.13}$	...	$0.38^{+0.21}_{-0.14}$	$0.31^{+0.15}_{-0.11}$
Ne/O	$0.51^{+0.21}_{-0.15}$	$0.86^{+0.28}_{-0.21}$	$0.48^{+0.22}_{-0.15}$	$0.44^{+0.18}_{-0.13}$
$O/H^0 \times 10^5$	6.7	...	7.4	26.8
$N/H^0 \times 10^5$	2.6	...	2.8	8.2
$Ne/H^0 \times 10^5$	3.4	...	3.5	11.9

[a] Value assumed from knot 4.

atoms, namely,

$$N(\mathrm{He}) = N_0(\mathrm{He}) + \frac{N_0(\mathrm{H}) - N(\mathrm{H})}{4}. \quad (2)$$

Introducing the initial and final ratios between helium and hydrogen, the ratio between the initial and final hydrogen number turns to be

$$\frac{N(\mathrm{H})}{N_0(\mathrm{H})} = \frac{1 + 4[N_0(\mathrm{He})/N_0(H)]}{1 + 4[N(\mathrm{He})/N(\mathrm{H})]}. \quad (3)$$

Assuming an initial ratio $N_0(\mathrm{He})/N_0(\mathrm{H}) = 0.10$ would mean that 95% of the original hydrogen has been converted into helium in knots J1 and J3, while in knot J4 it amounts to 90%.

In Table 4 we have also included the abundances of heavy elements relative to the initial hydrogen abundance. We can express this as

$$\frac{N(\mathrm{X})}{N_0(\mathrm{H})} = \frac{N(\mathrm{X})}{N(\mathrm{H})} \left\{ \frac{1 + 4[N_0(\mathrm{He})/N_0(H)]}{1 + 4[N(\mathrm{He})/N(\mathrm{H})]} \right\}. \quad (4)$$

Expressed in this way, oxygen and nitrogen abundances in knots J1 and J3 are an order of magnitude lower than the typical values found in PNs, while J4 has a more normal content of heavy elements. The ratio N/O is $\sim$0.35, similar to the value reported for type II PNs.

Neon is also low in knots J1 and J3, but only a factor of 3 lower than the average value found for PNs. The ratio Ne/O is relatively high, with an average value $\sim$0.5. In knots J2 and J4, the lines [Ne IV] $\lambda\lambda$4715, 4725 are prominent, and an abundance calculation of Ne^{3+}/H^+ is unreliable. This is also the case for the central region of A78 (Manchado, Pottasch, & Mampaso 1988). It seems that the temperature must be higher in the Ne^{3+} zone.

If we had adopted the extinction correction ($c_{\mathrm{H}\beta} = 0.4$) of JF83, some changes would be expected in the above results. First, we would find higher[4] electron temperatures ($T_e \sim$ 17,000 K), and consequently heavy-element abundances would be lower by a factor of 1.5. The ratio N/O would decrease to $\sim$0.3, and helium abundances would fall by $\sim$10%.

For the surrounding nebula, we computed N_e(rms) from the Hβ flux according to expression (V.5) in Pottasch (1984, p. 106):

$$N_e(\mathrm{rms})\epsilon^{1/2} = 2.74 \times 10^4 \left[\frac{F(\mathrm{H}\beta)t^{0.88}}{\theta^3 d} \right]^{1/2}, \quad (5)$$

where ϵ is the filling factor, F(Hβ) is the dereddened flux of the Hβ line in units of 10^{-11} ergs cm^{-2} s^{-1}, $t = T_e/10{,}000$, θ is the angular radius in arcseconds, and d is the distance in kiloparsecs. The derived density is $\sim$20 cm^{-3} ($\epsilon = 0.7$), the ionized mass being $\sim 0.1 M_\odot$. Since no diagnostic lines for the electron temperature are present in these spectra, we have not been able to calculate them. In order to investigate the chemical abundances of the inner and outer shells, these were computed for electron temperatures ranging from 10,000 to 20,000 K. As chemical abundances—especially of the O^{++} ion—are very sensitive to electron temperature, only broad limits can be established.

The envelopes that surround the central part of A30 are of very high excitation. Apart from Hα and Hβ, only strong He II λ4686 and [O III] lines are detected. Neither lines from low ionization stages nor He I are seen in the spectra. Although this information might seem scanty, some conclusions can be drafted.

The lack of low-ionization lines and the high He II λ4686 to Hβ ratio ($\gtrsim$1.1) indicate that the nebula is density-bounded and optically thin in the hydrogen Lyman continuum. On the assumption that the nebula is a sphere filled with gas of constant density and that the stellar spectrum resembles a blackbody spectrum, we used the code CLOUDY (Ferland 1990) to compute the nebular spectrum. Using the nebular radius, we adjusted a stellar temperature of 100,000 K to match the observed spectrum. The choice of a blackbody law for the stellar spectrum is not a critical point, since the nebula is strongly density-bounded and the stellar spectrum below 54 eV has practically no effect at all on the nebular spectrum.

The He^{++} abundances are $\sim$0.13, without showing any difference between the inner and outer parts of the envelope. Since there is no indication of He I lines, only upper limits can be established. Taking into account the uncertainty in the flux measurements, an intensity of the He I λ5876 line less than 10% that of Hα would elude detection. Therefore, $He^+/H^+ \leq 0.02$ and the total helium abundances are found to be between 0.13 and 0.15.

Finally, spectra from the inner and outer parts of the envelope differ clearly. The ratio I([O III λ5007])/I(Hβ) in the inner region is 2.5 times greater than in the outer envelope. Assuming a constant oxygen abundance and the same ionization fractions, material in the inner region would present a higher electron temperature (by 5000 K) than in the outer region. However, it seems unlikely that the same ionization fractions should apply in both regions, since the high T_{eff} of the central star would ionize the oxygen at higher stages of ionization than O^{++} near the star (no emission from low ionic species, such as O^+, is detected). Therefore, we should expect to detect less [O III] emission from the inner regions. An alternative explanation is that some of the hydrogen-poor material of the knots is being driven into the inner envelope (Borkowski et al. 1993), enhancing the abundances of He, C, N, O, and Ne. It is still difficult to explain how the small amount of mass contained in the inner knots [M(envelope)/M(inner knots) $\sim$ 400] might contaminate the outer envelope, and, in fact, we do not find any difference in the helium abundances between the inner and the outer envelope to support this idea. It is unclear whether the higher I([O III] λ5007)/I(Hβ) ratio in the inner envelope is a result of differential enrichment or of the existence of a different excitation mechanism from the one in the outer part of the envelope.

4. A58

4.1. *Spectral Analysis*

Figure 7 (Plate 15) shows the spectral region of the two-dimensional spectrum around the Hα and [N II] lines. Emission of hydrogen lines is clearly blueshifted at the central knot position, thus indicating that hydrogen is present. Our spectra also show blueshifted emission of the [O III], [O II], [O I], [S II], and He I lines.

One-dimensional spectra of the outer nebula and the central knot are presented in Figure 8. The blue and red parts of the spectra are shown separately. A magnification

[4] Surprisingly, after correcting their reddening data, JF83 found a value of $T_e \sim$ 15,000 K, similar to ours.

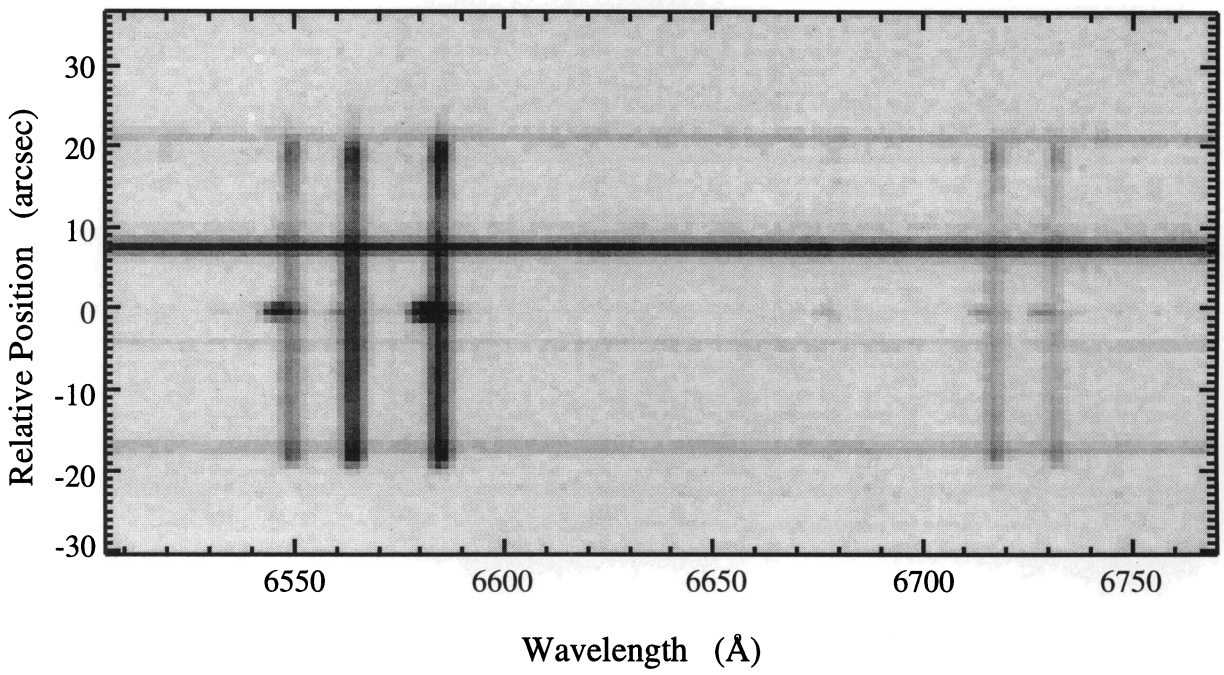

FIG. 7.—Two-dimensional spectrum of A58 showing the spectral region of the [N II], Hα, and [S II] lines. Emission from the central knot appears clearly blueshifted with respect to the nebular emission.

GUERRERO & MANCHADO (see 472, 717)

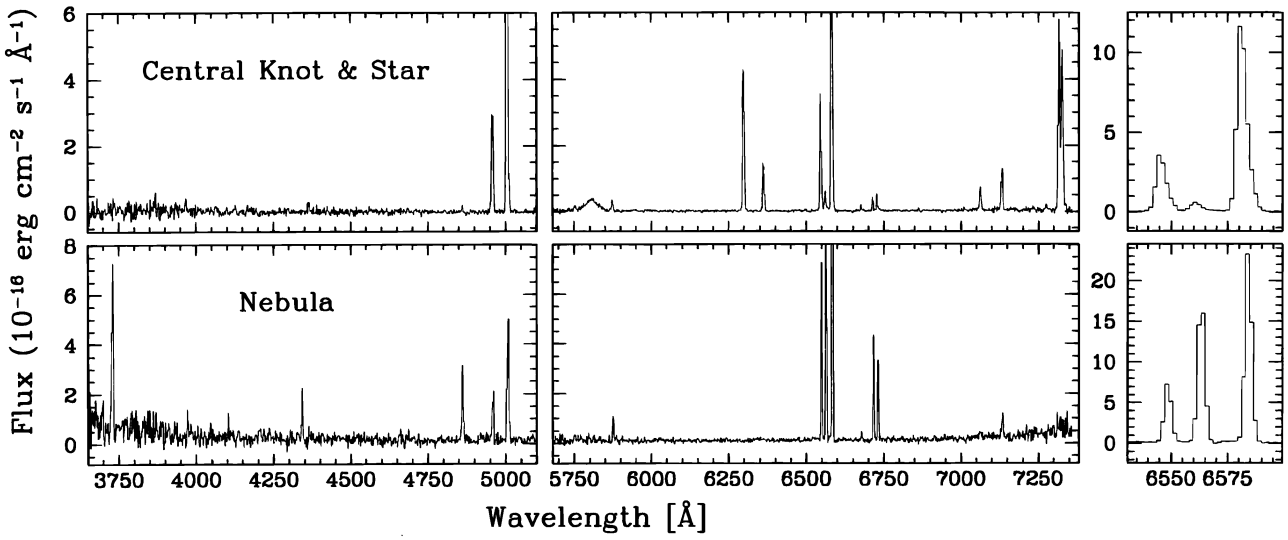

FIG. 8.—Individual spectra of the central knot and the envelope of A58

of the Hα region has also been included, in order to compare the emission from the nebula and the central knot. The nebular contribution to the central knot emission has been removed by fitting a continuum to the spatial profile of the lines.

The central knot spectrum is not only characterized by poor hydrogen emission; it also exhibits bright [O I] λλ6300, 6363 and [O II] λλ7320, 7330 lines, as well as the characteristic C IV Wolf-Rayet feature at 5801, 5812 Å corresponding to the star. Although our spectral resolution does not allow an accurate estimate of the width of the lines, they are broader than in the nebular spectrum (a fact previously reported by Pollacco et al. 1992, who found broad [N II] lines). The FWHM corresponds to ~ 180 km s^{-1} for the Hα and [N II] lines and is lower for the [S II] lines (FWHM ~ 100 km s^{-1}), while [O III] lines have a FWHM of ~ 230 km s^{-1}. However, we are able to measure the velocity of the knot, relative to the nebular lines of A58, for different emission lines. A shift of ~ -140 km s^{-1} is found for various lines (Hα, He I, [N II], [S II], and [O I]), while a different shift is found for the [O III] line (~ -100 km s^{-1}).

The nebular spectrum is of low excitation, the high-excitation He II λ4686 line being 10 times lower than Hβ. The [O III] λ5007 Å line is only 1.6 times Hβ.

TABLE 5

INTRINSIC LINE INTENSITY RATIOS FOR A58

Line	$f(\lambda)$	Knot and Star	Main Nebula
[O II] λ3727	0.265	...	89 ± 31
[Ne III] λ3869	0.228	...	...
Hε + [Ne III] + He I λ3970	0.203	...	7.0 ± 2.6
Hδ λ4101	0.172	...	7.5 ± 2.6
Hγ λ4340	0.129	...	15.5 ± 4.3
He II λ4686	0.042	...	3.8 ± 1.0
Hβ λ4861	0.000	...	35.1 ± 5.7
[O III] λ4959	−0.023	464 ± 69	23.0 ± 3.6
[O III] λ5007	−0.034	1448 ± 4.7	57 ± 8
[N II] λ5755	−0.191	30.8 ± 2.8	...
C IV λ5801+12 WR	−0.201	331 ± 22	...
He I λ5876	−0.216	54 ± 4.3	6.7 ± 0.8
[O I] λ6300	−0.285	482 ± 14	...
[O I] λ6364	−0.294	162 ± 5	...
[N II] λ6548	−0.321	350 ± 9	42.8 ± 0.6
Hα λ6563	−0.323	100	100
[N II] λ6584	−0.326	1144 ± 28	130 ± 1
He I λ6678	−0.338	...	2.1 ± 0.4
[S II] λ6717	−0.343	24.6 ± 1.5	22.3 ± 0.5
[S II] λ6731	−0.345	37.2 ± 1.9	17.8 ± 0.5
[Ar V] λ7008	−0.380	3.6 ± 1.6	...
He I λ7065	−0.386	79 ± 4	...
[Ar III] λ7136	−0.395	166 ± 7	10.1 ± 0.8
[O II] λ7320	−0.420	654 ± 30	...
[O II] λ7330	−0.420	548 ± 25	...
F(Hα)[a]		5.9	67.9

[a] Dereddened fluxes in units of 10^{-16} ergs cm^{-2} s^{-1}.

4.2. *Line Intensity Ratios*

The un-dereddened intensity ratios relative to the intensity of Hα (=100.0) and the Hα fluxes are shown in Table 5. Extinction correction was performed by comparing the measured and theoretical (Brocklehurst 1971) Hα/Hβ ratio in the nebula. The interstellar extinction coefficient obtained was $c_{H\beta} = 0.29$. There is some evidence that extinction in the central knot is higher than in the outer nebula, but the uncertainty in the measured Hα/Hβ ratio is so large than we have decided to adopt the same value as in the surrounding nebula. A similar effect has been observed in A30, where no extinction seems to affect the outer nebula, while the inner knots show evidence of reddening. These facts can be related to the high IR flux measured in these objects (Pottasch et al. 1986), pointing to the presence of large amounts of dust in the central regions.

4.3. *Physical Properties and Chemical Abundances*

In order to calculate the plasma diagnostic parameters and chemical abundances of A58, a similar procedure to that used for A30 was applied. As regards the central knot, the density-sensitive [S II] λλ6717, 6731 doublet lines yield an electron density of 2600 cm^{-3}, a value similar to that reported in the central knots of A30. The electron temperature was computed using the ratio between the [N II] auroral λ5755 and the nebular lines λλ6548, 6584. The value found is T_e[N II] = 12,450 ± 350 K. For the outer nebula, the electron density estimate is N_e[N II] = 200 cm^{-3}. Owing to the lack of electron temperature diagnostic lines in this region, T_e was assumed to be 10,000 K.

Table 6 shows the physical parameters and chemical abundances found in the knot and in the outer nebula. The helium-to-hydrogen ratio is extremely high in the central knot, reaching a value of 1.24, which, according to equation (3), means that 75% of the initial hydrogen has been burned into helium. In the outer nebula we found typical abundances of a type I PN, with helium and nitrogen abundances enhanced (He/H ∼ 0.15, N/O ∼ 0.7).

The oxygen abundances are unreliably high in the central knot, and the reason for this is that forbidden lines are excited by shocks. In fact, even assuming that hydrogen has been reduced by a factor of 4, the high [O I] λ6300 and [O II] λλ7320, 7330 to Hα ratios found [I(6300)/I(Hα) ∼ 5, I(7320+7330)/I(Hα) ∼ 12] provides definitive evidence to support the presence of excitation by shocks in the central knot of A58 (Hartigan, Raymond, & Hartmann 1987).

TABLE 6

PHYSICAL PARAMETERS AND ABUNDANCES OF A58

Plasma Diagnostics and Chemical Abundances	Knot	Main Nebula
N_e [S II]	2600^{+400}_{-300}	200
t [N II]	1.245 ± 0.035	1.0[a]
$O^{++}/H^+ \times 10^5$	51 ± 14	6.0 ± 0.8
$O^+/H^+ \times 10^5$	1067 ± 214	9.7 ± 3.0
$O^0/H^+ \times 10^5$	130 ± 16	...
$O/H \times 10^5$	...	16.7 ± 4.0
$N^+/H^+ \times 10^5$	38 ± 4	7.10 ± 0.05
$N/H \times 10^5$	...	12.2 ± 6.0
$S^+/H^+ \times 10^7$	36 ± 5	26.6 ± 0.6
$S/H \times 10^7$	...	177
$Ar^{++}/H^+ \times 10^6$	21 ± 4	2.6 ± 0.2
$Ar^{4+}/H^+ \times 10^6$	1.5 ± 0.7	...
$Ar/H \times 10^6$	...	4.9
He^+/H^+	1.24 ± 0.15	0.137 ± 0.004
He^{++}/H^+	...	0.013 ± 0.005
He/H	1.24 ± 90.15	0.150 ± 0.009
H^+/O^+	...	$0.73^{+0.30}_{-0.16}$

[a] Assumed value.

4.4. *The Central Knot*

The central star (V605 Aql) of A58 experienced a nova-like event in 1919 (Lundmark 1921). At that time, material was presumably ejected from the central star and has been expanding ever since. However, the central knot could not have been spatially resolved previously. The high spatial resolution of the images obtained at the NOT (the FWHM of stars in the field is 0.″55) have allowed us to discern the existence of diffuse emission in the line [N II] λ6584 surrounding the brighter central region. Figure 9*a* shows a contour of the central knot of A58 in this line. The point-spread function of the central region has a stellar profile with a FWHM of 0.″7. According to Bedding & Zijlstra (1994), a diameter of 1.″0 can be computed using as a model a disk of uniform surface brightness.

In order to show more clearly the diffuse emission surrounding the central part, the point-spread function was calculated from stars in the field and subsequently subtracted. The result is shown in Figure 9*b*. Emission is found on both sides of the center at P.A. ∼220°, although it is brighter and more extended toward the southwest (radius ∼1.″4). A peak appears in this direction at ∼0.″75 that can be interpreted as an ejected knot.

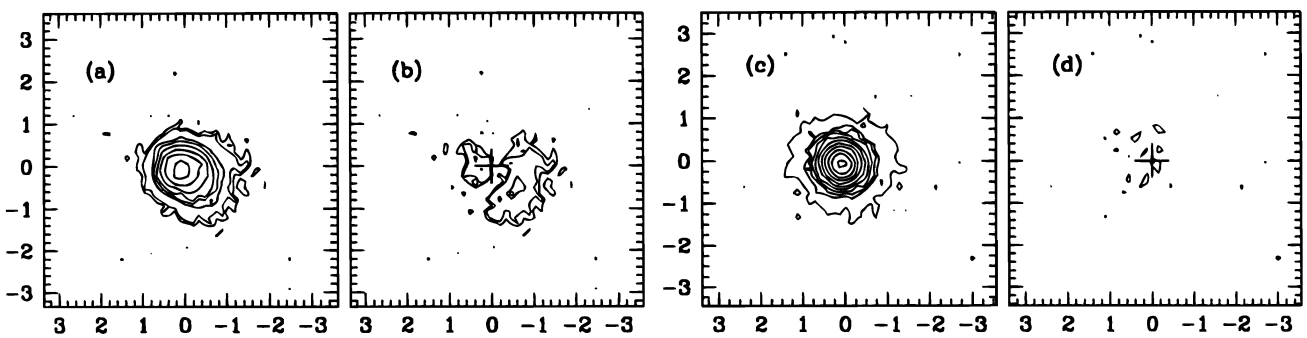

FIG. 9.—Contour profiles of the central knot of A58 (*a*) before and (*b*) after subtracting the central starlike emission. For comparison, the same is shown for a field star in (*c*) and (*d*). No significant residuals are found in the last case. The minimum contour is 3σ over the background, and the contours are logarithmic, separated by a factor of 1.5 in intensity.

TABLE 7

CHEMICAL ABUNDANCES IN HYDROGEN-DEFICIENT KNOTS

Object	He/H	O/H_0	N/H_0	N/O	X	Y	Z_O	Z_N
A30 knot J1	7.7	6.7×10^{-5}	2.6×10^{-5}	0.39	0.031	0.967	7.5×10^{-4}	2.6×10^{-4}
A30 knot J2	>1.0	...	...	...	...	...	...	...
A30 knot J3	7.4	7.4×10^{-5}	2.8×10^{-5}	0.38	0.032	0.966	8.4×10^{-4}	2.8×10^{-4}
A30 knot J4	4.0	2.7×10^{-4}	8.2×10^{-5}	0.31	0.059	0.937	3.0×10^{-3}	8.2×10^{-4}
A58 knot[a]	1.2	8.7×10^{-3}	3.1×10^{-4}	0.04	0.160	0.795	3.2×10^{-2}	1.0×10^{-3}
A78 knot[b]	2.7	5.6×10^{-3}	1.5×10^{-2}	2.7	0.062	0.666	0.122	0.106
IRAS 14514−5258[c]	>0.4	$>2.2 \times 10^{-3}$	...	...	...	...	...	...
Sun	0.10	8.5×10^{-4}	1.0×10^{-4}	0.12	0.704	0.282	9.6×10^{-3}	9.9×10^{-4}

[a] Nitrogen and oxygen abundances calculation affected by shock excitation.
[b] Manchado, Pottasch, & Mampaso 1988.
[c] Manchado, García-Lario, & Pottasch 1989.

Through their high-resolution spectra, Pollacco et al. (1992) proposed the existence of a collimated outflow of which only the front side is observed while the rear side remains partially obscured. Since the expansion velocity of the ejected material (blueshifted by 120 km s^{-1} with respect to the nebula), and its age (76 yr) are known, some relations can be worked out on the assumption that the material expands at a constant velocity. Let i be the outflow inclination angle with the line of sight, D the distance to the nebula in kiloparsecs, and v the expansion velocity in kilometers per second. Then

$$\tan i = 1.48 \frac{D}{3.8} \frac{120}{v}, \qquad (6)$$

and an inclination of 56° results at a distance of 3.8 kpc (Maciel 1984). The size of the ejected outflow is 1.7×10^{-2} pc.

5. DISCUSSION

5.1. *Chemical Composition*

The chemical abundances of the central knots and the outer envelopes of the hydrogen-poor PNs A30 and A58 have been studied in §§ 3 and 4. Here we include the results for other objects belonging to this group, such as A78 and IRAS 14514−5258. Table 7 contains the chemical composition of the central knots of A30, A58, and A78, and of the PN IRAS 14514−5258, as well as the chemical abundances relative to the original hydrogen according to equation (4). The chemical composition of the Sun has been included for comparison (Grevesse & Anders 1991).

The main characteristic of these objects is the extreme hydrogen deficiency in the knots located near their respective central stars. Assuming an initial helium-to-hydrogen ratio of 0.10 for the progenitor star, it means that a significant fraction of the original hydrogen (between 75% and 95%) has been converted into helium. Therefore, the extreme chemical composition of these knots indicates that we are observing material which has been processed through complete nuclear burning of hydrogen, rather than enriched material as the result of a dredge-up process.

It is interesting to note that the abundances of heavy elements are, however, very different among these objects. While A30 knots J1 and J3 (the polar knots) exhibit the highest He/H ratio (~7.5), they are deficient in heavy elements if referred to the original amount of hydrogen ($O/H_0 \sim 7 \times 10^{-5}$, $N/H_0 \sim 3 \times 10^{-5}$) (Grevesse & Anders 1991). In contrast, A78 central regions are overenriched both in helium and heavy elements (He/H ~ 2.7, $O/H_0 \sim 6 \times 10^{-3}$, N/O ~ 2.7). The A58 central knot has a lower He/H ratio, while it has the highest O/H_0 and the lowest N/O ratio. However, the reader should bear in mind that there is likely to be shock excitation of the plasma in this region.

There is a trend that indicates that helium and oxygen abundances are anticorrelated. The high oxygen and nitrogen abundances found in A58 and A78 might indicate that a portion of the recently formed helium was converted into fresh oxygen and nitrogen. This process does not seem to have occurred in A30 knots J1 and J3. If we apply equation (4) to helium, we infer higher He/H_0 in knots J1 and J3 (~0.34, 0.36 being a total conversion) than in A58 and A78 (~0.30). The difference found can account for the higher oxygen and nitrogen abundances detected in the central regions of these nebulae. Therefore, although all these objects have high helium abundances, the exact chemical composition differs among them, thus suggesting different physical conditions at the time when the helium shell flash occurred and during the born-again phase.

Another interesting point is the chemical segregation among knots J1 and J3 in A30 (the polar knots) and knot J4, which exhibits lower He/H (~4.0) and higher heavy-element abundances. It confirms the chemical segregation between knots J3 and J4 previously suggested by JF83. Bearing in mind the kinematics of these knots, knots J2 and J4 were ejected first, forming a ring or torus which collimated the polar knots J1 and J3 ejected afterward. The ejection of material at different times would lead to the chemical segregation described, via a fast change of surface abundances.

The outer parts of these nebulae have hydrogen-rich chemical compositions. The helium abundance of the A58 outer envelope is He/H = 0.15, while the N/O ratio is ~0.7. This means a high mass (~5 $M_\odot$) progenitor star (Becker & Iben 1980). In the case of A30, the outer nebula helium abundances (He/H ~ 0.13–0.15) are not so extreme and we do not have information on the N/O ratio.

5.2. *The Evolutionary Path of Hydrogen-poor PNs*

It is clear that the knots near the nuclei of the hydrogen-poor PNs are due to a secondary ejection of material which occurred recently The current interpretation for this peculiar kind of object is that they are "born-again" AGB stars (Iben et al. 1983); that is, they were PNNs that suffered a final thermal flash. During the thermal pulse, the hydrogen-rich material, confined to a thin surface layer of the star, is partially absorbed by the convective shell produced by the

TABLE 8

EXPANSION AGE AND INTERSHELL TIME LAP

		Inner Knots			Outer Nebula			
Object	Distance (kpc)	Diameter (arcsec)	V_{exp} (km s^{-1})	Age (yr)	Diameter (arcsec)	V_{exp} (km s^{-1})	Age (yr)	$\Delta\tau_{Intershell}$ (yr)
A30	1.7[a]	10–14	25–50[b]	750–2200	130	40[c]	13000	1100–12000
A50	3.8[d]	...	...	75[e]	40	31[f]	23000	23000
A78[g].....	1.6	72	43	8400	125	30	34000	25000

[a] Cahn, Kaler, & Stanghellini 1992.
[b] Jacoby & Chu 1989.
[c] Reay, Atherton, & Taylor 1983..
[d] Maciel 1984.
[e] Lundmark 1921.
[f] Pollacco et al. 1992.
[g] Ho et al. 1996.

helium burning. Consequently, any later ejecta of material are highly processed. At present the PNNs are evolving again to higher surface temperatures. They are in fact Wolf-Rayet stars, as in the case of A30, which shows a high temperature and luminosity, while A58 has lower luminosity (magnitude ~ 20) and presumably lower effective temperature.

If the distance to the PN is known, the kinematical age of the outer shells and the recently ejected knots can be established roughly from their expansion velocities and radius or distance to their central stars. Using the more recent data, these values are summarized in Table 8. The time elapsed between the ejection of the nebular envelope and the ejection of the central knots is 12,000 yr for A30, 23,000 yr for A58, and 25,000 yr for A78. Although this period of time depends on the mass of the PNN (e.g., more massive PNNs evolve faster, since they burn their hydrogen envelopes at higher rates), it is especially dependent on the mass of the hydrogen-rich envelope of the PNN prior to the helium shell flash (Iben 1984), and on the mass-loss rate during the post-AGB phase (Schönberner 1979). Accordingly, PNNs which retained more massive hydrogen-rich envelopes will evolve more rapidly and suffer a post-AGB helium flash over a shorter timescale. Since Table 8 reveals that in A30 the time elapsed between the formation of the nebula and the ejection of the central knots is roughly half the time for A58 and A78, the envelope mass of A30 should be the most massive. It is interesting to note that the He/H ratio found in A30 is far higher than in the other nebulae. A likely connection between the helium and oxygen enrichment in the central knots, and the time required for the late helium shell flash and the envelope mass on the post-AGB phase can be speculated on. In fact, the time that the model spends as a born-again AGB star (Iben 1984) increases linearly with the envelope mass. We proposed that a longer period of time in the born-again AGB phase would allow the convective mixing to take place over longer timescales, thus increasing the efficiency of the whole process and the amount of pure helium brought up to the surface of the star.

A30, A58, and A78 are different views of the same evolutionary process. A PN is ejected, and under certain conditions the central star experiences a thermonuclear runaway after 10,000–20,000 yr, like those experienced by V605 Aql 75 yr ago. The material just ejected expands and is excited via shocks, due to the high velocities and densities involved, as is occurring in the central knot of A58. The energy deposited inside the nebula by this shock and the variations that follow in the central star's spectrum will eventually excite the PN itself, which explains the different excitation detected between A58 (typical of a very old PN) and A30 and A78, where most of the helium is found as He^{++}. At the same time, some material from the central knots may diffuse (Borkowski et al. 1993) from the innermost regions, swept up by the strong stellar wind. As a result of this, the inner regions of the envelope might suffer from contamination from hydrogen-exhausted material. The final scenario might be a very hot hydrogen-deficient central star surrounded by an old, albeit very excited, PN, as is the case of K1-27 (Rauch, Köppen, & Werner 1994).

Although the theory explains the hydrogen-deficient composition of the inner knots, there are some difficult points. First, it is hard to find an interpretation for the chemical segregation among the knots of A30, since, theoretically, the hydrogen-exhausted material is ejected in a short timescale (1000–4000 yr) during the born-again AGB phase (Iben 1984). A fast change of the stellar surface chemical abundances is needed in order to modify the chemical composition of the material ejected, as well as the addition of angular momentum to allow an equatorial ring to form and to collimate the polar ejection. The scenario proposed by Soker & Livio (1994) (i.e., an evolved nebula flowing back and undergoing accretion by the central star) can account for the presence of polar knots if angular momentum is present in the nebula. This idea needs further investigation in order to find out whether different chemical compositions are allowed.

Second, theoretical predictions on this subject (Schönberner 1979) indicate that post-AGB stars of less than 0.6 $M_\odot$ may only experience a late helium shell flash and undergo the born-again process. However, the chemical abundances of the outer nebulae of A58 and the mass of the central star of A30 and A78 ($\sim 0.7\ M_\odot$; Heap 1982) suggest that their progenitors were originally more massive stars.

5.3. *The Frequency of Hydrogen-deficient PNs*

The frequency of hydrogen-deficient PNs is very low. Only five PNs (over ~ 1500) are known to share their peculiar features. There are different reasons that account for this fact. First, the hydrogen-poor knots contain a small amount of mass ($\lesssim 10^{-4}\ M_\odot$ in A30 knots) and have high velocities (~ 150 km s^{-1} in A58). It is therefore reasonable to assume that in a short timescale they expand and dilute into the surrounding nebula. According to the dynamical ages of the knots in the objects that we have studied, they

will be not visible in a few thousand years (2000–3000 yr). Compared with the timescale of PNs, this means that we are only able to observe between 1/10 and 1/15 of them ($\sim$10%).

However, the small frequency of detections is not accounted for. In addition, hydrogen-deficient PNs would be very exotic events occurring to stars which follow very particular evolutionary tracks. Iben (1984) explored the probabilities that the central star of a PN evolved into a "born-again" phase. Depending on the mass-loss rates assumed during the post-AGB evolution, between 10% and 20% of these stars experienced a late helium shell flash.

Since the chemical abundances have been calculated for a sample of $\sim$300 PNs (Aller & Keyes 1987; Köppen, Acker, & Stenholm 1991; Perinotto 1991), the number of hydrogen-deficient PNs expected in this sample is $300 \times 0.10 \times 0.15 \simeq 4$. This value is in agreement with the number of known objects.

6. SUMMARY

We have studied the chemical abundances of the central knots of A30 and A58 in detail, as well as their surrounding envelopes. Dynamical ages of the outer envelopes and stellar parameters have also been considered in this investigation.

Given that A30 and A58 are objects whose inner knots are almost hydrogen-exhausted, a special effort has been made to measure accurately the emission from the hydrogen lines. In particular, we found that previous studies of A30 overestimate the content of hydrogen due to the contribution of the He II series lines to the lines of the Balmer series. A chemical segregation among the polar knots J1 and J3 and the equatorial knots J2 and J4 is confirmed, the former having higher helium abundances. In A58 we found hydrogen emission in the inner knot that had not been reported previously, allowing the hydrogen depletion to be determined. We also came across evidence of shock excitation.

There is a significant trend towards finding higher oxygen abundances in those knots where helium abundances are lower. This might indicate the existence of processes which burn helium into heavier elements. In addition, higher helium abundances seem to be related to the shorter time elapsed between the formation of the nebulae and the helium flash, which theoretically means higher envelope mass on the post-AGB phase. We suggest that the higher He/H and lower oxygen abundances are related to the fact that they remain for a longer period on the born-again AGB phase, which allows greater amounts of completely processed material to be dredged up to the surface. This point would require further theoretical investigation.

Another interesting point refers to the chemical abundances found in the outer nebulae of A58, which are typical of type I PNs, with He/H $\sim$ 0.15 and N/O $\sim$ 0.7. This definitely indicates that the progenitor of A58 could not be a low-mass star ($\sim 1.5\ M_{\odot}$).

The IAC80 is operated on the island of Tenerife by the Instituto de Astrofisica de Canarias in the Spanish Observatorio del Teide. The 2.5 m Nordic Optical Telescope is operated on the island of La Palma by the Lund Observatory in the Spanish Observatorio del Roque de los Muchachos of the Instituto de Astrofisica de Canarias. We thank Artemio Herrero and Romano Corradi for helpful discussions, and Antonio Aparicio for helping in the calculation of the point-spread function described in § 4.4. We are also grateful to Andrea Preite-Martinez for the use of his program on abundance calculations, and to Monica Murphy, who read the manuscript. This research was partially funded through grant PB94-1108 from the Dirección General de Investigación Científica y Técnica of the Spanish Ministerio de Educación y Ciencia.

REFERENCES

Aller, L. H., & Keyes, C. D. 1987, ApJS, 65, 405
Becker, S. A., & Iben, I., Jr. 1980, ApJ, 237, 111
Bedding, T. R., & Zijlstra, A. A. 1994, A&AS, 283, 955
Borkowski, K. J., Harrington, J. P., Blair, W. P., & Bregman, J. D. 1994, ApJ, 435, 722
Borkowski, K. J., Harrington, J. P., Tsvetanov, Z., & Clegg, R. E. S. 1993, ApJ, 415, 47
Brocklehurst, M. 1971, MNRAS, 153, 471
Burstein, D., & Heiles, C. 1982, AJ, 87, 1165
Butler, K., & Mendoza, C. 1984, MNRAS, 208, 17P
Cahn, J. H., Kaler, J. B., & Stanghellini, L. 1992, A&AS, 94, 399
Clegg, R. E. S. 1987, MNRAS, 229, 31P
Cohen, M., Hudson, H., O'Dell, S., & Stein, W. A. 1977, MNRAS, 181, 233
Dinerstein, H. L., & Lester, D. F. 1984, ApJ, 281, 702
Ferland, G. J. 1990, in HAZY: A Brief Introduction to CLOUDY, Version 76.03
Gillett, F. C., Neugebauer, G., Emerson, J. P., & Rice, W. L. 1986, ApJ, 300, 722
Grevesse, N., & Anders, E. 1991, in Solar Interior and Atmosphere (Tucson: Univ. Arizona Press), 1227
Harrington, J. P. 1986, in Workshop on Model Nebulae, ed. D. Péquignot (Paris: Observatoire de Paris), 81
Hartigan, P., Raymond, J., & Hartmann, L. 1987, ApJ, 316, 323
Hazard, C., Terlevich, R., Morton, D. C., Sargent, W. L. W., & Ferland, G. 1980, Nature, 285, 463
Heap, S. R. 1982, in IAU Symp. 99, Wolf-Rayet Stars: Observations, Physics, Evolution, ed. C. W. H. de Loore & A. J. Willis (Dordrecht: Kluwer), 423
Ho, C.-H., Chu, Y.-H., Manchado, A., Chiueh, T.-H., & Jacoby, G. H. 1996, in preparation
Hummer, D. G., & Storey, P. J. 1987, MNRAS, 224, 801
Iben, I., Jr. 1984, ApJ, 277, 333
Iben, I., Jr., Kaler, J. B., Truran, J. W., & Renzini, A. 1983, ApJ, 264, 605
Jacoby, G. H. 1979, PASP, 91, 754
Jacoby, G. H., & Chu, Y.-H. 1989, in IAU Symp. 131, Planetary Nebulae, ed. S. Torres-Peimbert (Dordrecht: Kluwer), 183
Jacoby, G. H., & Ford, H. C. 1983, ApJ, 266, 298 (JF83)
Kingsburgh, R. L., & Barlow, M. J. 1994, MNRAS, 271, 257
Köppen, J., Acker, A., & Stenholm, B. 1991, A&A, 248, 197
Lundmark, K. 1921, PASP, 33, 314
Maciel, W. J. 1984, A&AS, 55, 253
Manchado, A., García-Lario, P., & Pottasch, S. R. 1989, A&A, 218, 267
Manchado, A., Guerrero, M. A., Stanghellini, L., & Serra-Ricart, M. 1996, The IAC Morphological Catalog of Northern Planetary Nebulae, in preparation
Manchado, A., Pottasch, S. R., & Mampaso, A. 1988, A&A, 191, 128
Mendoza, C. 1983, in IAU Symp. 103, Planetary Nebulae, ed. D. R. Flower (Dordrecht: Reidel), 43
Oke, J. B. 1974, ApJS, 27, 21
———. 1990, AJ, 99, 1621
Perinotto, M. 1991, ApJS, 76, 687
Pollacco, D. L., Lawson, W. A., Clegg, R. E. S., & Hill, P. W. 1992, MNRAS, 257, 33P
Pottasch, S. R. 1984, Planetary Nebulae (Dordrecht: Reidel)
Pottasch, S. R., Mampaso, A., Manchado, A., & Menzies, J. 1986, in IAU Colloq. 87, Hydrogen-deficient Stars and Related Objects, ed. K. Hunger, D. Schönberner, & R. Kameswara (Dordrecht: Reidel), 359
Rauch, T., Köppen, J., & Werner, K. 1994, A&A, 286, 543
Reay, N. K., Atherton, P. D., & Taylor, K. 1983, MNRAS, 203, 1079
Schönberner, D. 1979, A&A, 79, 108
Seitter, W. C. 1987, ESO Messenger, 50, 14
Soker, N., & Livio, M. 1994, ApJ, 421, 219
Stone, R. P. S. 1977, ApJ, 218, 767